Elastocapillary Crease

Qihan Liu, Tetsu Ouchi, Lihua Jin, Ryan Hayward, and Zhigang Suo

Phys. Rev. Lett. **122**, 098003 — Published 7 March 2019

DOI: 10.1103/PhysRevLett.122.098003

Elastocapillary crease

Qihan Liu[1]*, Tetsu Ouchi[2]*, Lihua Jin[3], Ryan Hayward[2]†, Zhigang Suo[1]‡

[1]John A. Paulson School of Engineering and Applied Sciences, Kavli Institute for Bionano Science and Technology, Harvard University, Cambridge, MA, 02138, USA

[2]Department of Polymer Science & Engineering, University of Massachusetts, Amherst, MA, 01003, USA

[3]Department of Mechanical and Aerospace Engineering, University of California, Los Angeles, CA 90095, USA

* These authors contributed equally to this work
† hayward@umass.edu
‡ suo@seas.harvard.edu

Abstract. A material under compression often forms creases. When the material is elastic and soft, the nucleation of creases depends on both elasticity and capillarity. Here we introduce a model of elastocapillary creases. The model assumes that the surface tension remains constant on the free surface, but may change upon self-contact. In particular, surface tension vanishes upon self-contact for a pristine surface of elastomers and gels. The model predicts that the nucleation of creases depends on the sizes of surface defects relative to the elastocapillary length, and happens over a well-defined range of strains, instead of a specific strain. The loss of surface tension upon self-contact lowers the energy barrier for nucleation, and widens the range of nucleation strains for materials of any thickness relative to the elastocapillary length. We test this model by conducting experiments with materials of various elastocapillary lengths, along with the data available in the literature.

Buckling a bar and blowing a bubble are elastic and capillary instabilities. Such familiar instabilities have long appealed to researchers for broad applications, as well as in developing concepts and tools for studying diverse—and often less familiar—instabilities in physics, chemistry, and biology. Much attention has also been paid to elastocapillary phenomena, such as fracture [1, 2], adhesion [3-9], cavitation [10-12], compositional patterns [13, 14], and morphological changes [9, 15-17].

This paper focuses on an elastocapillary instability: creases nucleated on soft and elastic materials under compression. Creases are commonly observed on rubbers [18, 19], gels [20-24], and soft tissues [25, 26]. Creases have been used to demonstrate stimuli-responsive displays of bimolecular patterns [27], stem cell differentiation [28], tunable adhesion [29], and switchable chemical patterns [30]. As ubiquitous as creases are, their scientific studies have led to conflicting findings. When capillary effect is weak, the crease forms at a specific strain [18, 31, 32], much below the critical strain predicted by a linear perturbation analysis [15]. When capillary effect is strong, one experiment reports that a crease nucleates near a specific strain predicted by the linear perturbation analysis [16], but another experiment reports that a crease extends at a specific strain much below the prediction of the linear perturbation analysis [17]. Existing models of elastocapillary creases characterize the strength of capillary effect by the elastocapillary length relative to the thickness of materials, but not relative to the size of defects [16, 17, 23]. The situation is puzzling, as one expects that the nucleation of creases is defect-sensitive.

Here we reconcile the conflicting findings by a new model of elastocapillary creases. The model assumes that surface tension is constant on the free surface, but may change upon self-contact. In particular, the surface tension vanishes upon self-contact for a pristine surface of elastomers and gels. The model predicts that the nucleation of creases depends on the sizes of surface defects relative to the elastocapillary length, and happens in a range of strains, instead of at a specific strain. The range of nucleation strains is well-defined by the thickness of materials

relative to the elastocapillary length. The loss of surface tension upon self-contact lowers the energy barrier for nucleation and widens the range of nucleation strains for materials of any sizes and elastocapillary lengths. We test this model by conducting experiments with materials of varying elastocapillary lengths, along with the data available in the literature.

We compare four models of surface instability (Fig. 1). Corresponding to each model is a distinct bifurcation diagram, which we sketch on the plane of the applied strain, ε, and the amplitude of deviation from the flat surface, A. The former is a loading parameter, and the latter a proxy for the state of deformation. A state of equilibrium corresponds to a point in the ε-A plane. A stable state corresponds to a local energy minimum, and an unstable state corresponds to a local energy maximum. As the applied strain changes, a sequence of equilibrium states forms a path. (The applied strain is the compressive displacement divided by the undeformed length of the sample. Unless otherwise stated, the material is taken to deform under the plane strain condition.) .) This paper focuses on the nucleation of creases, not the subsequent evolution of the creases. The theory assumes that the soft material is elastic, and neglects any migration of solvent in the material.

In the absence of surface tension, the onset of wrinkle and the onset of crease are two distinct elastic instabilities. A wrinkle is a smooth undulation of the surface, the calculated strain for the onset of the wrinkle is $\varepsilon_w = 0.46$ [15], and the wrinkled state is unstable [33] (Fig.1a). A crease is a self-contact of the surface, the calculated strain for the onset of crease is $\varepsilon_c = 0.35$ [31, 32], and the creased state is stable [34] (Fig.1b). Since crease has lower critical strain and is stable, crease is the only observable surface instability.

The model of elastic creases makes a remarkable prediction: creases nucleate at a specific strain. This prediction is understood as follows. The model assumes neo-Hookean elasticity, which well describes the soft elastic materials used in experiments (elastomers and gels) at the level of strain for crease nucleation. The model has a single material parameter, the shear modulus, and has no material-specific length. The size of the specimen is irrelevant to the

onset of a crease, because the crease can be arbitrarily small. Consequently, the nucleation of the crease is scale-free, fully determined by the local state of strain. The model has no other dimensionless parameter, and predicts that the nucleation strain is independent of material, specimen geometry, and surface defects.

In the presence of surface tension, a material-specific length emerges: the elastocapillary length γ/μ, where γ is the surface tension and μ is the shear modulus. We neglect the change in surface tension due to deformation. For a defect-free elastic film of thickness H in the stress-free state, the elastocapillary number $\gamma/\mu H$ and the applied strain ε are the only dimensionless parameters in this elastocapillary boundary value problem.

We assume that the surface tension of a soft material does not change with deformation, but may change upon self-contact [35]. For an elastomer, segments of a polymer chain far away from crosslinkers behave as if in a polymer melt. Upon self-contact, the polymer segments mix across the contact. For a highly swollen gel, the surface tension is dominated by that of the solvent [8, 40]. Upon self-contact, the solvent mixes across the interface. Consequently, a clean surface of an elastomer or a gel completely loses surface tension upon self-contact. A contaminated surface may retain some surface tension upon self-contact. As will become clear, the loss of surface tension upon self-contact profoundly affects the nucleation of creases.

We first consider a model of elastocapillary creases with constant surface tension γ everywhere (Fig. 1c). When the surface is curved with a local radius of curvature R, the surface tension produces the Laplace pressure $p = \gamma / R$. If the self-contact retains the surface tension, a crease must have a rounded tip since a sharp crease tip would result in a diverging Laplace pressure. The size of the round tip must scale with the only length scale, γ/μ. Consequently, an infinitesimal crease is no longer possible. Accordingly, the previously derived bifurcation to form sharp-tip crease of arbitrarily small size does not exist anymore. The surface can only become unstable and bifurcates into a wrinkle at a higher critical strain ε_w. As we will show

later by finite element simulation, this wrinkle is unstable, corresponding to the green portion of the post-bifurcation path in Fig.1c. The neighboring peaks contact each other when the amplitude of the wrinkle, A, is comparable to the elastocapillary length, γ/μ. The self-contact stabilizes the undulated surface and turns the post-bifurcation path around (Fig.1c red line). We identify the point where the post-bifurcation path turns around as the critical point of crease, with the strain ε_c. In the presence of surface tension, creasing and wrinkling are no longer different instabilities, but are different stages of the same instability.

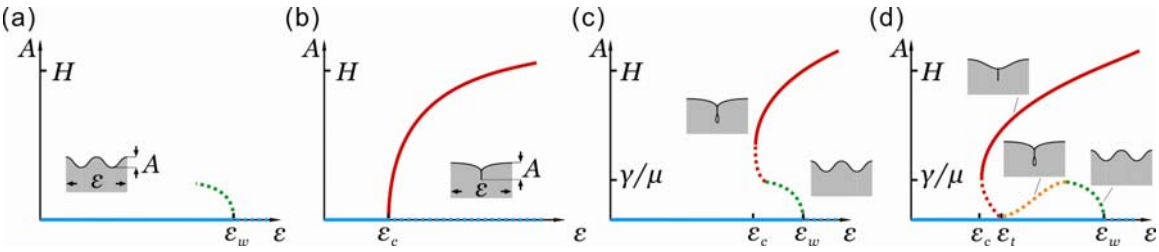

FIG.1. Bifurcation diagrams of four models of instability. In the bifurcation diagrams, different colors mean different surface morphologies. Solid lines mean stable states and dotted lines mean unstable states. (a) Elastic wrinkles. (b) Elastic creases. (c) Elastocapillary creases of constant surface tension. (d) Elastocapillary creases with vanishing surface tension upon self-contact.

We next consider the model of elastocapillary creases with vanishing surface tension upon self-contact (Fig. 1d). Before the surface self-contacts, the two models of elastocapillary creases have the same behavior. Once the surface self-contacts, the loss of surface tension in the second model zips up the contact. Since the size of the crease tip scales with γ/μ, the vanishing surface tension implies a crease of a sharp tip. A triple line forms where the free surface and the self-contact meet. Since the free surface has constant surface tension and the self-contact has vanishing surface tension, the balance of forces at the triple line requires that the free surface be flat and that the self-contact be vertical to the free surface. Since the zipped crease can continuously shrink to infinitesimal size, a surface with infinitesimal crease is on the post-bifurcation path. As an infinitesimal crease only infinitesimally perturbs the free energy from a

flat state, the post-bifurcation path representing crease (Fig.1d red) and the fundamental path representing the flat surface (Fig.1d blue) must touch. Although an infinitesimal crease and the flat surface have the same free energy at the touch point (at strain ε_t), the touch point is not a bifurcation point because surface tension imposes an energy barrier between the flat state and the creased state. This is similar to the first order phase transition observed in water boiling, where the liquid phase and the vapor phase have the same free energy at boiling temperature, but a vapor bubble has to overcome an energy barrier to nucleate from the liquid phase. We again identify the point where the post-bifurcation path becomes stable as the critical point of crease.

We compute the bifurcation diagrams of the two models of elastocapillary creases using the finite element method [41]. For example, consider the computed bifurcation diagrams for the elastocapillary number $\gamma/\mu H = 0.25$ (Fig.2a,b). The wrinkle forms at $\varepsilon_w = 0.55$, in agreement with the analytical result obtained from the linear perturbation analysis [43]. The wrinkle is subcritical. For the model of constant γ, the self-contact point and the critical point of crease coincide at $\varepsilon_c = 0.51$, although the two points may separate for other values of the elastocapillary number (Fig.S2). For the model with $\gamma_{con} = 0$, the post-bifurcation path of the zipped crease (Fig.2b red) touches the horizontal line of the fundamental path. The critical strain for crease predicted by the model of elastocapillary creases with vanishing surface tension upon self-contact is $\varepsilon_c = 0.39$, which is much below the value 0.51 predicted by the model of elastocapillary creases with constant surface tension and is somewhat above the value 0.35 predicted by the model of elastic creases.

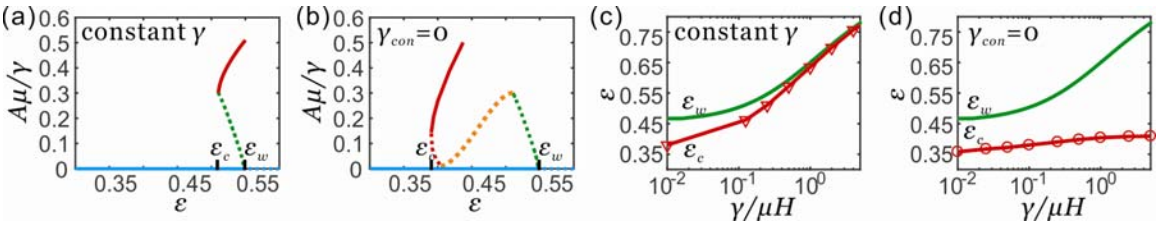

FIG.2. Finite element simulation of the two models of elastocapillary creases. Bifurcation diagrams for the elastocapillary crease of (a) constant surface tension, and (b) vanishing surface tension upon self-contact. The zipping portion of the post-bifurcation path (orange) is not simulated, but is schematically drawn to connect the simulated parts of the post-bifurcation path. Critical strains as functions of the elastocapillary number predicted by the model of elastocapillary crease of (c) constant surface tension, and (d) vanishing surface tension upon self-contact.

To appreciate the significance of the loss of surface tension upon self-contact, we compare the critical strains of the two models of elastocapillary creases (Fig.2c,2d). The critical strain of wrinkle ε_w is the same for both models, and is calculated analytically [43]. However, the critical strain of crease ε_c differs for the two models. When $\gamma/\mu H \to 0$, both elastocapillary models recover the predictions of the models of elastic crease and elastic wrinkle. But as $\gamma/\mu H$ increases, the model of constant surface tension predicts increasingly high ε_c, close to ε_w, because the surface tension greatly penalizes the increased surface area in the crease. The difference between ε_c and ε_w is less than 0.02 for $\gamma/\mu H > 1$. For the model of vanishing surface tension upon self-contact, ε_c also increases with $\gamma/\mu H$, but asymptotes to a value of 0.41. The asymptote exists because when the surface tension is high, the free surface becomes hard to deform and effectively remain flat as the crease forms (Fig.S3). Forming a crease while maintaining a flat free surface is a pure elastic problem independent of the elastocapillary number $\gamma/\mu H$. A comparison of the two models shows that the loss of surface tension upon self-contact does not change the gap between ε_c and ε_w when $\gamma/\mu H$ is small, but greatly widens the gap when $\gamma/\mu H$ is large.

Our model predicts that defects affect nucleation strains (Fig. 3). In the presence of a

defect of size d, a new dimensionless number emerges, the elastocapillary number of the defect, $\gamma/\mu d$, in addition to the other two dimensionless numbers, the elastocapillary number of the specimen, $\gamma/\mu H$, and the applied strain, ε. If $d << \gamma/\mu$, the surface tension smoothens the defect, so that the surface only becomes unstable near ε_w, and then snaps into a crease. If $d >> \gamma/\mu$, the strain at the defect is much higher than the overall strain in the material, so that the defect can be compressed into self-contact at a relatively low overall strain, and deepens substantially near ε_c. For a defect of arbitrary size, the nucleation strain of a crease should be bounded by these two limits, ε_c and ε_w.

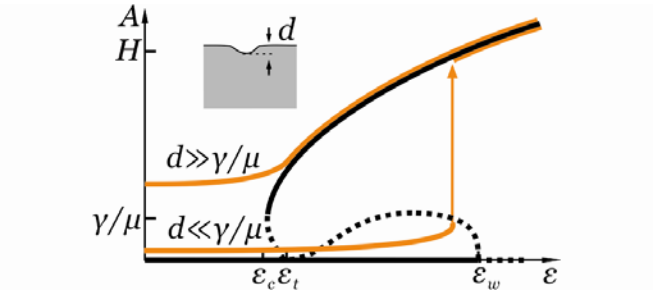

FIG.3. The observed nucleation strain for a crease depends on the size of a defect relative to the elastocapillary length. (a) If $d << \gamma/\mu$, a crease nucleates near ε_w. (b) If $d >> \gamma/\mu$, a crease nucleates near ε_c.

We characterize the strength of capillary effect by comparing the elastocapillary length both to the thickness of the specimen, $\gamma/\mu H$, and to the size of the defect, $\gamma/\mu d$. The former sets the range of nucleation strains, and the latter the observed nucleation strain. A stiff elastomer, of $\gamma = 10$ mN/m and $\mu = 1$ MPa, has an elastocapillary length of $\gamma/\mu = 10$ nm. It is common to have $d \gg 10$nm and $H \gg 10$nm, so that the model of elastic creases prevails: creases nucleate on the stiff elastomer at the specific strain of $\varepsilon_c = 0.35$. By contrast, a soft hydrogel, of

$\gamma = 70$ mN/m and $\mu = 100$ Pa, has an elastocapillary length of $\gamma/\mu = 0.7$ mm. Defects of sizes smaller than the elastocapillary length are obtained with common laboratory procedures, so that the nucleation of creases is defect-insensitive, at a specific strain ε_w, set by the value of $\gamma/\mu H$. Between the two extreme cases, a hydrogel, of $\gamma = 70$ mN/m and $\mu = 10$ kPa, has an elastocapillary length of $\gamma/\mu = 7$ μm. Defects of sizes both larger and smaller than the elastocapillary length are readily available, so that the nucleation of creases is defect-sensitive, and happens in a range of strains. Whereas constant surface tension causes a wide range of nucleation strains only for small values of $\gamma/\mu H$ (Fig. 2c), the loss of surface tension causes a wide range of nucleation strains for all values of $\gamma/\mu H$ (Fig. 2d).

We experimentally verify our model of elastocapillary creases [44]. We cure a polyacrylamide hydrogel, thickness H = 1 mm, shear modulus between 0.16 kPa and 8.7 kPa, on a pre-stretched polyurethane 'mounting layer'. The surface tension of the hydrogel is taken as that of the precursor solution, which is about 65 mN/m. Consequently, the elastocapillary length γ/μ varies from 7.3 μm to 0.4 mm (Table S2), and the elastocapillary number $\mu/\gamma H$ of the specimen varies from 0.0073 to 0.4. The pre-stretch is later released to compress the hydrogel layer, while the surface of the hydrogel is monitored by a high-speed camera. The nucleation of each crease is then identified by analyzing the video recording. All the experiments are conducted in a humidity chamber to limit the drying of the hydrogel.

We observed crease nucleation from both visible defects (Fig.4a, Video S1) and invisible defects (Fig.4b, Video S2). The visible defects were larger than the invisible defects. The visible defects led to lower nucleation strain, in accord with our model. Our experiments, as well as the data in the literature [16, 17], did not contaminate the surfaces. Consequently, we compare the experimentally measured nucleation strains to our theoretical predictions of ε_w and ε_c according to the model of vanishing surface tension upon contact (Fig. 4c). Since the strain in the hydrogel film is not homogeneous after the first nucleation of the crease or at the edge of the

hydrogel, we only plot the nucleation strain of the first crease that nucleates from the center of each sample. Our finite element simulations are under the plane strain condition, but our experiments are conducted under uniaxial force. We convert the nucleation strain under the plane strain condition to that under uniaxial force [45].

As predicted by our model, for a given value of $\gamma/\mu H$, creases nucleated in a range of strains, rather than at a specific strain, and the distribution was confined between ε_w and ε_c (Fig. 4c). As $\gamma/\mu H \to 1$, more creases nucleated near ε_w, probably because naturally occurring defects were much smaller than the film thickness of 1 mm, so that $d << \gamma/\mu$. The nucleation strains reported in Mora et al. [16] are close to higher limit ε_w, possibly because the soft hydrogels they used (12 – 4200 Pa) result in elastocapillary lengths much larger than defects. Chen et al [17] reported the channeling strain in an elastomer with thickness gradient. The data are close to the lower limit ε_c because channeling creases come from existing creases, which act as large defects.

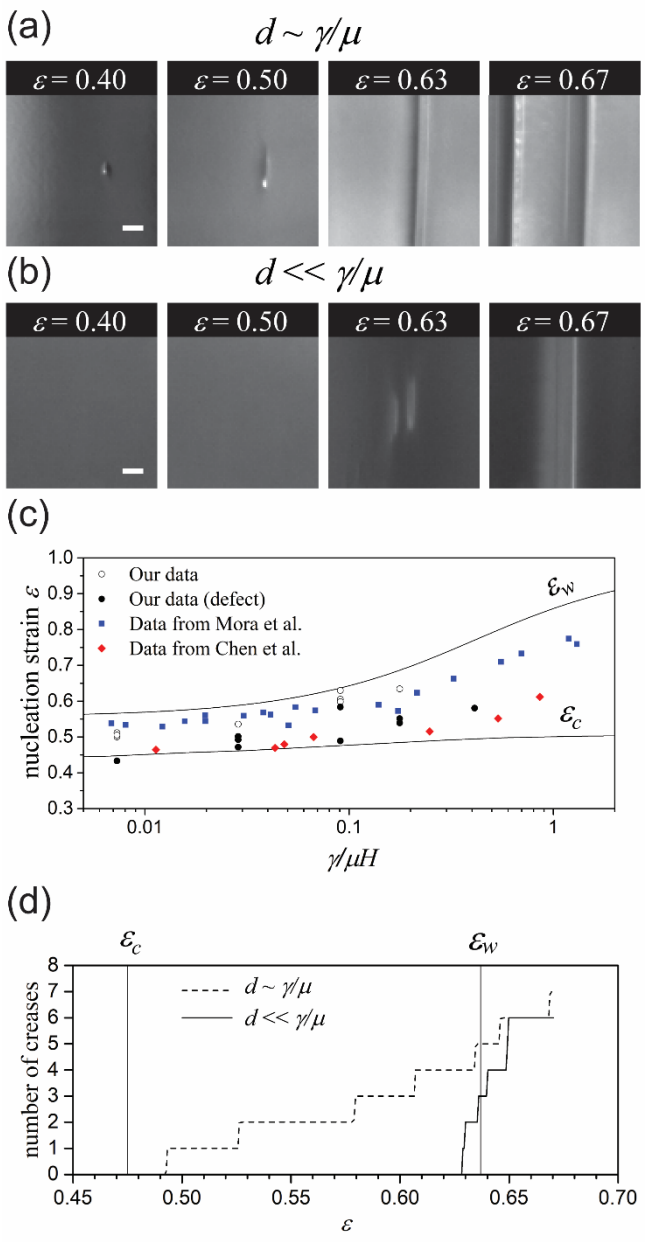

FIG.4. Defect sensitivity is demonstrated by comparing (a) a sample with visible defects $d \sim \gamma/\mu$, and (b) crease nucleated from the center part of the sample without visible defects $d << \gamma/\mu$. For both samples, γ/μ = 0.091 mm and H =1.0 mm. The scale bar is 0.3 mm. (c) Experimentally measured nucleation strains are compared with theoretically predicted range of nucleation strains assuming vanishing surface tension upon self-contact. In the legend, (defect) means a first crease formed from the center of the sample associated with a visible defect. (d)

The nucleation history of the samples of (a) and (b).

After the nucleation of the first crease, more creases nucleate as the sample is further compressed (Fig. 4d). Since the strain on the hydrogel is no longer homogeneous after the nucleation of the first crease, the exact nucleation strain of these subsequent creases cannot be determined from our experiment. We may nevertheless make some qualitative observation based on the distribution of the nucleation strains. For $H = 1.0$ mm and $\gamma/\mu = 90\mu$m, defects larger than 90 μm occur rather scarcely. Consequently, even if we have visible defects (Fig.4a, video S1), few creases nucleate from defects of $d \sim \gamma/\mu$ at a strain much below ε_w while most creases nucleate from defects of $d << \gamma/\mu$, at a strain close to ε_w. On the other hand, if there is no visible defect, which means that all the defects have size $d << \gamma/\mu$, all creases nucleate almost simultaneously near ε_w (Fig.4b, video S2). Since the earlier forming crease would locally relax the compressive strain, we always observe the last few creases nucleating above ε_w of the mounting layer. This observation should not be taken as a violation of the theory.

In summary, we have developed a model of elastocapillary crease, and tested the model with experiments reported here and available in the literature. So long as surface defects have a statistical distribution and can be both larger and smaller than the elastocapillary length, creases nucleate in a range of strains, instead of at a specific strain. The range of nucleation strain is well-defined for a given material thickness relative to the elastocapillary length. The loss of surface tension upon self-contact lowers the energy barrier for nucleation, and widens the range of nucleation strains for materials of any thickness relative to the elastocapillary length.

Acknowledgements. The work was supported by the National Science Foundation (NSF) through MRSEC (DMR-14-20570) at Harvard, and through Grant No. DMR-13-09331 at UMass.

References

1. Griffith, A.A. and M. Eng, *VI. The phenomena of rupture and flow in solids*. Phil. Trans. R. Soc. Lond. A, 1921. **221**(582-593): p. 163-198.
2. Bonn, D., et al., *Delayed fracture of an inhomogeneous soft solid*. Science, 1998. **280**(5361): p. 265-267.
3. Obreimoff, J., *The splitting strength of mica*. Proc. R. Soc. Lond. A, 1930. **127**(805): p. 290-297.
4. Johnson, K.L., K. Kendall, and A. Roberts, *Surface energy and the contact of elastic solids*. Proc. R. Soc. Lond. A, 1971. **324**(1558): p. 301-313.
5. Gösele, U. and Q.-Y. Tong, *Semiconductor wafer bonding*. Annual Review of Materials Science, 1998. **28**(1): p. 215-241.
6. Hui, C., et al., *Constraints on microcontact printing imposed by stamp deformation*. Langmuir, 2002. **18**(4): p. 1394-1407.
7. Bico, J., et al., *Adhesion: elastocapillary coalescence in wet hair*. Nature, 2004. **432**(7018): p. 690.
8. Chakrabarti, A. and M.K. Chaudhury, *Direct measurement of the surface tension of a soft elastic hydrogel: exploration of elastocapillary instability in adhesion*. Langmuir, 2013. **29**(23): p. 6926-6935.
9. Style, R.W., et al., *Elastocapillarity: Surface tension and the mechanics of soft solids*. Annual Review of Condensed Matter Physics, 2017. **8**: p. 99-118.
10. Gent, A. and D. Tompkins, *Nucleation and growth of gas bubbles in elastomers*. Journal of applied physics, 1969. **40**(6): p. 2520-2525.
11. Zimberlin, J.A., et al., *Cavitation rheology for soft materials*. Soft Matter, 2007. **3**(6): p. 763-767.
12. Cristiano, A., et al., *An experimental investigation of fracture by cavitation of model elastomeric networks*. Journal of Polymer Science Part B: Polymer Physics, 2010. **48**(13): p. 1409-1422.
13. Kern, K., et al., *Long-range spatial self-organization in the adsorbate-induced restructuring of surfaces: Cu {100}-(2× 1) O*. Physical review letters, 1991. **67**(7): p. 855.
14. Lu, W. and Z. Suo, *Dynamics of nanoscale pattern formation of an epitaxial monolayer*. Journal of the Mechanics and Physics of Solids, 2001. **49**(9): p. 1937-1950.
15. Biot, M.A., *Surface instability of rubber in compression*. Applied Scientific Research, Section A, 1963. **12**(2): p. 168-182.
16. Mora, S., et al., *Surface instability of soft solids under strain*. Soft Matter, 2011. **7**(22): p. 10612-10619.
17. Chen, D., et al., *Surface energy as a barrier to creasing of elastomer films: An elastic analogy to classical nucleation*. Physical review letters, 2012. **109**(3): p. 038001.
18. Gent, A. and I. Cho, *Surface instabilities in compressed or bent rubber blocks*. Rubber Chemistry and Technology, 1999. **72**(2): p. 253-262.
19. Southern, E. and A. Thomas, *Effect of constraints on the equilibrium swelling of rubber vulcanizates*. Journal of Polymer Science Part A: General Papers, 1965. **3**(2): p. 641-646.
20. Tanaka, T., et al., *Mechanical instability of gels at the phase transition*. Nature, 1987. **325**(6107): p. 796.
21. Drummond, W.R., et al., *Surface instabilities during swelling of pH-sensitive hydrogels*. Journal of controlled release, 1988. **7**(2): p. 181-183.
22. Tanaka, H. and T. Sigehuzi, *Surface-pattern evolution in a swelling gel under a geometrical constraint: Direct observation of fold structure and its coarsening dynamics*. Physical Review E, 1994. **49**(1): p. R39.
23. Yoon, J., J. Kim, and R.C. Hayward, *Nucleation, growth, and hysteresis of surface creases on swelled polymer gels*. Soft Matter, 2010. **6**(22): p. 5807-5816.
24. Ghatak, A. and A.L. Das, *Kink instability of a highly deformable elastic cylinder*. Physical review letters, 2007. **99**(7): p. 076101.
25. Jin, L., S. Cai, and Z. Suo, *Creases in soft tissues generated by growth*. EPL (Europhysics Letters), 2011. **95**(6): p. 64002.
26. Tallinen, T., et al., *On the growth and form of cortical convolutions*. Nature Physics, 2016. **12**(6): p. 588.
27. Kim, J., J. Yoon, and R.C. Hayward, *Dynamic display of biomolecular patterns through an elastic creasing instability of stimuli-responsive hydrogels*. Nature materials, 2010. **9**(2): p. 159.

28. Saha, K., et al., *Surface creasing instability of soft polyacrylamide cell culture substrates*. Biophysical journal, 2010. **99**(12): p. L94-L96.
29. Chan, E.P., J.M. Karp, and R.S. Langer, *A "self-pinning" adhesive based on responsive surface wrinkles*. Journal of Polymer Science Part B: Polymer Physics, 2011. **49**(1): p. 40-44.
30. Yoon, J., et al., *Local switching of chemical patterns through light-triggered unfolding of creased hydrogel surfaces*. Angewandte Chemie, 2012. **124**(29): p. 7258-7261.
31. Hohlfeld, E. and L. Mahadevan, *Unfolding the sulcus*. Physical review letters, 2011. **106**(10): p. 105702.
32. Hong, W., X. Zhao, and Z. Suo, *Formation of creases on the surfaces of elastomers and gels*. Applied Physics Letters, 2009. **95**(11): p. 111901.
33. Cao, Y. and J.W. Hutchinson, *From wrinkles to creases in elastomers: the instability and imperfection-sensitivity of wrinkling*. Proc. R. Soc. A, 2012. **468**(2137): p. 94-115.
34. Cai, S., et al., *Creasing instability of elastomer films*. Soft Matter, 2012. **8**(5): p. 1301-1304.
35. See Supplemental Material [url] for a discussion on the continuum theory of elastocapillarity, which includes Refs. [9,35-39]
36. Rubinstein, M. and R. Colby, P*olymers physics*. Vol. 767. 2003: Oxford Oxford, UK.
37. Flory, P.J. and J. Rehner Jr, S*tatistical Mechanics of Cross-Linked Polymer Networks I. Rubberlike Elasticity*. The Journal of Chemical Physics, 1943. 1**1(**11): p. 512-520.
38. Flory, P.J. and J. Rehner Jr, S*tatistical mechanics of cross-linked polymer networks II. Swelling*. The Journal of Chemical Physics, 1943. 1**1(**11): p. 521-526.
39. Zhao, X., W. Hong, and Z. Suo, E*lectromechanical hysteresis and coexistent states in dielectric elastomers*. Physical review B, 2007. 7**6(**13): p. 134113.
40. Style, R.W., et al., U*niversal deformation of soft substrates near a contact line and the direct measurement of solid surface stresses*. Physical review letters, 2013. 1**10(**6): p. 066103.
41. See Supplemental Material [url] for a description of the finite element method to compute the bifurcation diagram, which includes Ref. [42]
42. Riks, E., T*he application of Newton's method to the problem of elastic stability*. Journal of Applied Mechanics, 1972. 3**9(**4): p. 1060-1065.
43. See Supplemental Material [url] for details on the linear perturbation analysis, which includes Ref. [16].
44. See Supplemental Material [url] for detailed description on experimental verification.
45. See Supplemental Material [url] for a discussion on generalized plane strain condition in elastocapillary problems, which includes Ref. [32].